



# CHORUS

This is the accepted manuscript made available via CHORUS. The article has been published as:

## Phase diagram of magnetic vortex dynamics

T. Y. Chen, A. T. Galkiewicz, and P. A. Crowell

Phys. Rev. B **85**, 180406 — Published 16 May 2012

DOI: [10.1103/PhysRevB.85.180406](https://doi.org/10.1103/PhysRevB.85.180406)

# Phase diagram of magnetic vortex dynamics

T. Y. Chen, A. T. Galkiewicz, and P. A. Crowell\*

*School of Physics and Astronomy, University of Minnesota, 116 Church St. SE, Minneapolis, MN 55455*

The dynamics of a magnetic vortex are influenced profoundly by non-linear effects at large and small amplitudes. For example, a strongly driven magnetic vortex is unstable with respect to internal deformation, leading to reversal of its core magnetization. At small amplitudes, a non-linear response is associated with pinning of the vortex core. Given these phenomena, there is an acute need for a global picture of vortex dynamics over a wide range of excitation amplitudes and frequencies. We have constructed a phase diagram of vortex dynamics in permalloy ( $\text{Ni}_{80}\text{Fe}_{20}$ ) disks by probing the response spectrum over four orders of magnitude in excitation power. We identify the boundary separating pinned and unpinned dynamics in a phase space of amplitude and frequency. Our approach allows for a highly quantitative analysis of the pinning potential for localized defects and can be used to trace the dynamics of a single vortex from deep in the pinning regime to the onset of core reversal.

PACS numbers: 75.78.-n, 75.78.Fg, 75.75.-c

A magnetic vortex represents the simplest possible domain structure. Although the magnetization circulates in the bulk of the disk, the most significant feature of a vortex is a core of diameter  $\sim 10$  nm, within which the magnetization rotates out of the disk plane, as shown schematically in Fig. 1(a). The lowest frequency excitation of a vortex is the gyrotropic mode, in which the vortex core circulates around its equilibrium position.<sup>1-3</sup> The gyrotropic mode in the linear regime is well-understood, with experiment, analytical theory, and micromagnetic simulation all showing that its frequency is determined by the geometric aspect ratio (thickness/diameter) of the disk.<sup>2,4-6</sup> Beyond the linear regime, two classes of non-linear dynamics have been reported. First, as the amplitude of vortex motion increases, higher order terms in the magnetostatic potential must be considered.<sup>7,8</sup> As the core velocity increases further, the vortex core deforms<sup>9,10</sup> and eventually the core polarity (direction of the perpendicular magnetization) reverses.<sup>11-14</sup>

Alongside these two classes of non-linear effects, vortex dynamics are profoundly affected by inhomogeneities in real materials. Previous studies have shown that when a vortex is pinned by a defect, the gyrotropic frequency increases as the amplitude approaches zero.<sup>15-20</sup> This implies the existence of a depinning threshold well below the onset of core reversal. The understanding of the depinning transition and the subsequent dynamics has been inhibited by the absence of an experimental probe with suitable sensitivity and dynamic range. The ideal probe would address the response of single vortex as a function of amplitude and frequency, with an amplitude range extending from the pinned regime up through the threshold for core reversal.

We present here a set of measurements on a single magnetic vortex over a large dynamic range, allowing us to construct a complete phase diagram of vortex dynamics. We identify three distinct regimes: the pinned vortex, a linear response regime corresponding to ordinary gyrotropic motion, and finally large amplitude dynamics accompanied by core reversal. In addition to core reversal at high amplitudes, a second class of non-linear dynamics is associated with the depinning transition, in which the response amplitude changes hysteretically as a function of the excitation amplitude. We show that the spectrum of the vortex oscillations near the depinning threshold can be used to measure the pinning energy. We also show that the pinning transition can be observed in the time domain as the amplitude of gyrotropic motion decreases. A simple model captures the physics of the depinning transition, including the existence of two metastable gyrotropic orbits (pinned and unpinned). The sensitivity and dynamic range of this approach in both the time and frequency domains make it suitable for testing models of magnetization dynamics in other systems, such as domain walls in nanowires.<sup>21-23</sup>

Time-resolved Kerr microscopy<sup>24</sup> is used to measure vortex dynamics in a single permalloy  $\text{Ni}_{80}\text{Fe}_{20}$  disk.<sup>2</sup> The disks discussed in this paper are  $2\ \mu\text{m}$  in diameter and  $50\ \text{nm}$  in thickness, patterned from sputtered films either on commercially polished single-crystal sapphire ( $\text{Al}_2\text{O}_3$ ) (0001) substrates with a  $30\ \text{nm}$  Cu buffer layer, or on Si substrates with a SiN buffer layer. The phase diagram presented in this paper is for the case of sapphire substrates with a Cu buffer layer, and similar phase diagrams were observed for the case of Si substrates with a SiN buffer layer. The sample substrate is polished to a thickness of  $50\ \mu\text{m}$  and positioned above the center conductor of a coplanar waveguide (CPWG) as shown in Fig. 1(b). The detailed experimental setup is described in Ref. 18. The important feature is the use of a continuous wave (CW) radio-frequency (RF) (0.001 - 1 GHz) source that is phase-locked to a sub-harmonic of the 76 MHz repetition rate of a pulsed Ti:sapphire laser. To obtain a polar Kerr signal, the linearly polarized laser pulse train is focused through an oil immersion objective to a spot with a full width at half maximum  $\sim 400\ \text{nm}$ . In this mode, the polar Kerr signal is acquired stroboscopically in a manner similar to a sampling oscilloscope, and purely stochastic effects are therefore averaged out. The CW signal can also be gated on and off, with the gating signal phase-locked to the laser, so that we can measure the response of the vortex core as it

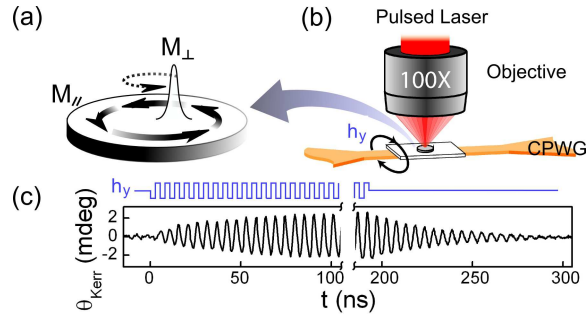


FIG. 1: (Color online) (a) Representation of a magnetic vortex. (b) Schematic diagram of the experiment. (c) Time scans of the polar Kerr signal excited by gated-CW excitation of a  $2 \mu\text{m}$  disk with an amplitude of 0.2 Oe and a frequency of 0.19 GHz. The excitation field is switched on at 0 nsec and is turned off at 190 nsec.

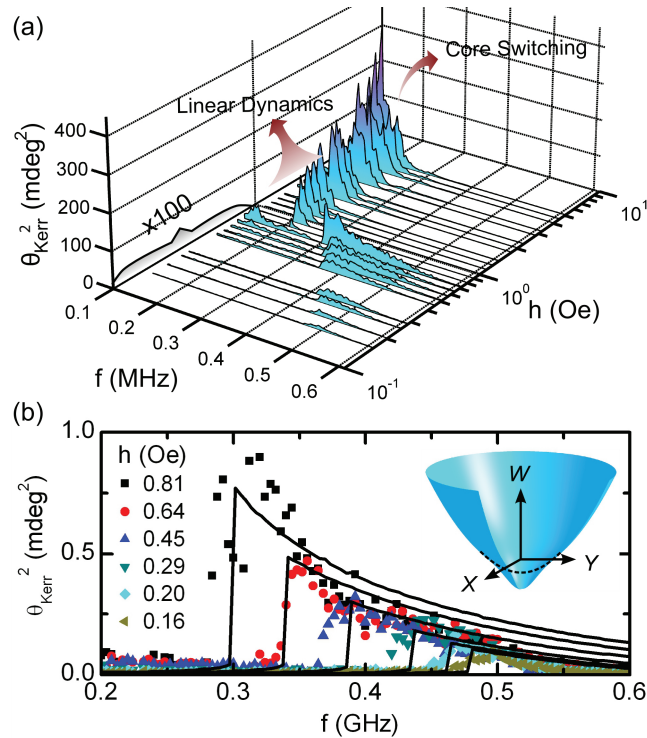


FIG. 2: (Color online) (a) Observed gyrotropic spectra of a  $2 \mu\text{m}$  disk excited by a CW magnetic field for amplitudes from 0.2 Oe to 5.1 Oe and frequencies up to 0.60 GHz. The position of the core is determined by the static external field of -50 Oe. Data at drive amplitudes below 0.8 Oe are multiplied by 100 for better visibility. (b) Gyrotropic spectra below 0.8 Oe from experiment (points) and numerical calculations (solid lines). Inset: Schematic of the potential energy described by Eq. 3, including a parabolic magnetostatic potential (dashed curve) and a Gaussian pinning potential.

either starts from rest or rings down after the excitation is turned off. A typical time scan obtained with gated-CW excitation is shown in Fig. 1(c), in which the polar Kerr signal  $\theta_{Kerr}$  shown is proportional to displacement of the vortex core. By switching the excitation field on and off, we can measure the gyrotropic motion during build-up, steady state motion, and ring-down.

As CW excitation is applied, the  $y$ -component of the motion of the vortex core is measured as a function of excitation frequency and amplitude, as shown in Fig. 2(a). For excitation fields between 1 and 2 Oe, the spectra show a single symmetric peak at 0.20 GHz. This is the ordinary gyrotropic mode, and both the lineshape and peak position indicate that the vortex dynamics are linear over this range.<sup>2,4-6</sup> The equation of motion for a vortex in this case can be derived from the Thiele equation<sup>4,6,25</sup> by making the assumption that the core moves as a rigid body:

$$\mathbf{G} \times \frac{d\mathbf{r}}{dt} - D \frac{d\mathbf{r}}{dt} - \frac{\partial W(\mathbf{r})}{\partial \mathbf{r}} = \mathbf{F}(t), \quad (1)$$

where  $\mathbf{r}$  is the displacement of the vortex core from its equilibrium position,  $\mathbf{G} = -2\pi p L M_s / \gamma \hat{\mathbf{z}}$  is the gyrovector,  $D = \alpha \pi M_s L (2 + \ln \frac{R}{R_c}) / \gamma$  is the damping constant with  $R_c = 0.68 L_e^{2/3} L^{1/3}$ ,  $W$  is the potential energy, and  $\mathbf{F}(t) = (\frac{2}{3} \pi M_s L R) \mathbf{h}(t) \times \hat{\mathbf{z}}$  is the time dependent excitation force. The parameter  $p = \pm 1$  is the vortex core polarization,  $L$  is the disk thickness,  $M_s$  is the saturation magnetization,  $\gamma$  is the gyromagnetic ratio,  $\alpha$  is the Gilbert damping parameter,  $R$  is the disk radius,  $L_e = \sqrt{2A/M_s^2}$  is the exchange length,  $A$  is the exchange constant, and  $\mathbf{h}(t)$  is the excitation field. The magnetostatic potential energy is approximated by a quadratic function  $W = kr^2/2$  near the center of the disk, and the vortex gyrotropic frequency is  $f_G = \omega_G/2\pi = k/2\pi G$ . The exact form of  $k$  depends on the boundary conditions, which previous measurements have shown to be closest to the ‘‘pole-free’’ (or ‘‘two-vortex’’) model of Guslienko.<sup>4</sup> In this case,  $k = (\frac{2}{3} M_s)^2 \pi L / \chi_0$ , and  $\chi_0 = R/10L$  is the vortex susceptibility.

For CW excitation fields above 2 Oe, the spectra become irregular and the measured amplitude saturates. As originally observed by Vansteenkiste *et al.*,<sup>10</sup> the assumption of a rigid core breaks down in this regime, and at the highest core velocities deformation of the vortex leads to the nucleation and subsequent annihilation of a vortex-antivortex pair, switching the core polarity.<sup>11</sup> The apparent splitting of gyrotropic mode spectra in this range seen in Fig. 2(a) results from the suppression of the average gyrotropic signal by successive core annihilation events.<sup>8,18</sup> In the high-amplitude regime, the time-dependent evolution of the signal after the rf excitation is turned on becomes non-monotonic, and suppression of the amplitude as well as phase modulation due to core reversal are observed.<sup>18</sup> Because of stochastic variations in the core-reversal process, however, only one or two reversal events can be observed directly. We can verify that core switching has occurred by comparing the phases of the gyrotropic motion before and after increasing the amplitude into the strongly non-linear regime and then decreasing it. We find that the final phase is opposite to the initial one in half of these cases. When the amplitude is maintained below the core reversal threshold, the phase (and hence the core polarity) never changes.

We now consider excitation fields below 1 Oe. At the lowest excitation amplitude (0.2 Oe), the spectrum of Fig. 2(a) shows a resonant peak at about 0.50 GHz, which is much higher than the gyrotropic mode frequency observed at higher amplitudes. As shown previously using pulsed excitation,<sup>15,17</sup> this enhancement of the gyrotropic frequency is due to pinning, and the limiting frequency at low amplitudes can be used to provide a map of pinning sites in the disk. The measured frequency reflects the local curvature of the effective potential  $W(r)$ . As the amplitude increases, the peak shifts to lower frequencies, but the weight at higher frequencies is preserved, and so the lineshape becomes triangular. Over a narrow range of driving amplitudes (0.8 to 1.0 Oe), the response amplitude increases by a factor of 10, and a narrow peak emerges at the gyrotropic frequency. We now consider how this behavior emerges from the dynamics of a driven vortex in the presence of a pinning site.

To model the spectrum in the presence of pinning, we assume a total potential

$$W(r) = \frac{1}{2}kr^2 + W_p(r). \quad (2)$$

The pinning potential  $W_p$  must have a local minimum (below that of the background magnetostatic potential) and must vanish for large  $r$ . This condition is satisfied by a Gaussian

$$W_p = -a \cdot \exp\left(\frac{-r^2}{2c^2}\right), \quad (3)$$

which captures both required features with only two parameters, a depth  $a$  and a width  $c$ , or full-width at half-maximum  $\text{FWHM} = c\sqrt{2\ln 2}$ . Due to the form of  $W_p$ , the equation of motion [Eq. (1)] becomes a two-dimensional non-linear system with explicit time-dependence. We solve this system numerically using typical material constants for  $\text{Ni}_{80}\text{Fe}_{20}$ , including  $M_s = 800 \text{ emu/cm}^3$ ,  $A = 1.05 \times 10^{-6} \text{ ergs/cm}$ , and the damping constant  $\alpha = 0.01$ . For a given choice of pinning center depth  $a$  and width  $c$ , we can solve for the spectrum at each driving amplitude. The results of this fit are shown in Fig. 2(b) as solid curves, which were obtained for  $a = 0.17 \text{ eV}$  and the FWHM  $c\sqrt{2\ln 2} = 7 \text{ nm}$ . The same approach can be applied to other pinning defects in the same disk. We find an average pinning energy  $0.7 \pm 0.2 \text{ eV}$  and pinning range  $16 \pm 3 \text{ nm}$  from six random pinning defects measured in this sample.

This model also provides a realistic picture of the depinning process and the dynamics above the depinning transition. The solutions of Eq. (1) with  $W$  of the form of Eq. (2) are orbits. At small amplitudes, the frequency of an orbit depends on  $r$ . For  $r > c$ , the frequency rapidly approaches the gyrotropic value 0.20 GHz. There is a well-defined boundary separating these two regimes. To obtain a global picture, it is instructive to represent the orbital amplitude as a contour plot in a parameter space of drive amplitude and frequency, as shown in Fig. 3(a) for the experiment and Fig. 3(b) for the numerical results. Note that the contours are shown for increasing amplitude, obtained by exciting the vortex starting from rest at each step of frequency and amplitude. The unpinned and pinned gyrotropic frequencies are indicated by vertical dashed lines. The sharp boundary separating the pinned and unpinned regimes as the drive amplitude increases is particularly evident for frequencies near the unpinned gyrotropic frequency. As

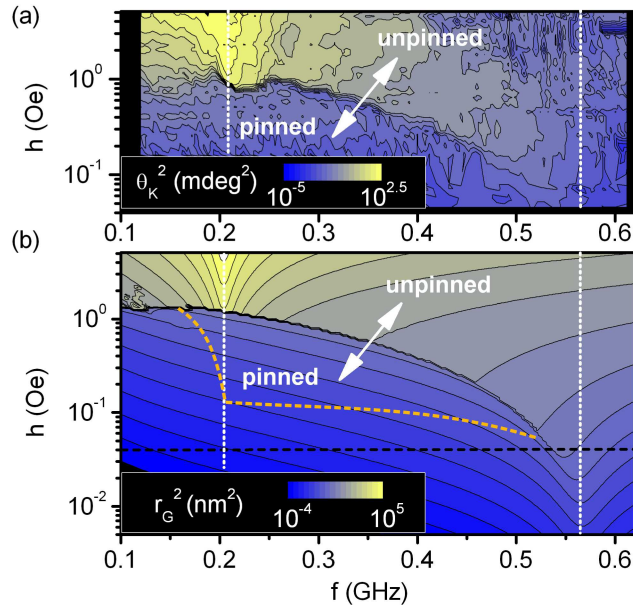


FIG. 3: (Color online) Gyrotropic response as a function of excitation amplitude and frequency for (a) experiment and (b) numerical calculations. The experimental parameter space is above the horizontal dashed line in (b). The color scale is logarithmic. The contours are shown for increasing amplitude. The dashed curve in (b) shows the lower boundary of the region in which two gyrotropic orbits exist.

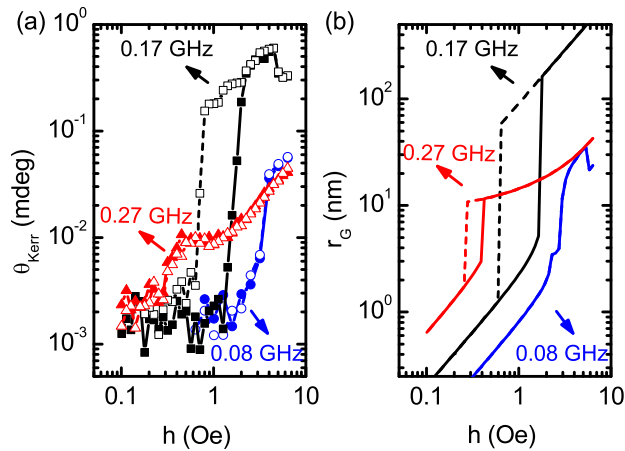


FIG. 4: (Color online)(a) Gyrotropic response versus excitation amplitude measured at 0.17 GHz ( $f_G$  of this disk), 0.08 GHz, and 0.27 GHz. Data taken on the increasing (decreasing) branch are shown using solid (dashed) lines and solid (open) symbols. (b) Numerical results for the same conditions as the experiment. The two branches correspond to two different vortex core orbits. Note that the error in the Kerr signal is approximately 2-3  $\mu\text{deg}$ . The step-like decrease in the 0.17 GHz experimental data at the highest amplitudes is due to core reversal.

discussed below, there are two metastable orbits in the depinning region, and either an external perturbation or thermal activation can allow the experimental system to jump to the outer (higher amplitude) orbit inside the metastable region, the lower boundary of which is shown as a dashed curve in Fig. 3(b).

To demonstrate this metastability, we carry out a monotonic sweep of the drive amplitude in both directions using a double modulation technique.<sup>26</sup> Experimental data are presented as solid (increasing) and dashed (decreasing) curves in Fig. 4(a), which shows the orbital amplitude measured as a function of excitation amplitude at three fixed excitation frequencies. The corresponding numerical results at these frequencies are shown in Fig. 4(b). The depinning with increasing excitation amplitude is easily observed. At the gyrotropic frequency (0.17 GHz for this slightly larger disk), both the experimental and the numerical results clearly show hysteresis in the depinning region, demonstrating the existence of two distinct orbits. At 0.08 GHz, no hysteresis is observed as expected. At 0.27 GHz, however, hysteresis

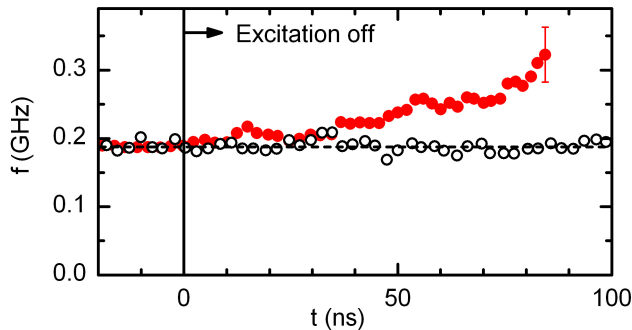


FIG. 5: (Color online) Frequency of the gyrotropic motion measured as a function of time when the equilibrium position is at a pinning site (filled symbols) or not at a pinning site (open symbols). The error bar represents an upper bound on the uncertainty in the frequency measurement, which is determined by the sampling rate of the time-domain signal.

is seen in the numerical results but not in the experiment, where the experimental resolution in Kerr signal is about 2-3  $\mu\text{deg}$ . This discrepancy is due to the presence of thermal activation in the experiment. In order to observe hysteresis, there must be a negligible probability for the core to jump from the pinned to the unpinned orbit on the time scale of the experiment, which is  $\sim 1$  sec. The energy difference  $\Delta E$  between the two orbits, calculated at the upper and lower boundaries of the coexistence region, is  $\sim 100$  eV at 0.17 GHz, but is only  $\sim 0.5$  eV at 0.27 GHz. The characteristic rate for thermally activated jumps to occur is  $f_0 \exp(-\Delta E/k_B T)$ , where  $f_0$  is the orbital frequency (the drive frequency). The calculated rate is insignificant at 0.17 GHz, but it is  $\sim 1 \text{ sec}^{-1}$  at 0.27 GHz, which is why hysteresis cannot be observed. As the depinning transition is approached from below, thermal activation becomes significant even at the gyrotropic frequency, which is why the depinning transition at the resonance in Fig. 3(a) dips slightly below the boundary seen in Fig. 3(b).

We now turn to the study of the pinning process in the time domain. We first excite a vortex in the linear regime, below the onset of core reversal. After the excitation field is switched off, the core spirals towards its equilibrium position, which may or may not be a pinning site. Both of these cases are shown in Fig. 5. The gyrotropic frequency  $f$ , determined from the time to complete each orbital cycle, is shown as a function of time in Fig. 5, with  $t = 0$  nsec corresponding to the time at which the excitation is turned off. In the unpinned case, the gyrotropic frequency remains fixed as expected. When, however, the equilibrium position is at a pinning site, the frequency is constant only up to a certain time, beyond which the frequency increases. For the case shown in Fig. 5, the core starts to interact with the pinning site after approximately 30 nsec.

The amplitude of the vortex motion versus time (data not shown) reveals the value of decay time  $\tau$ , which along with  $f$  can be used to determine the Gilbert damping parameter  $\alpha$ , given that  $f \cdot \tau = [\pi(2 + \ln \frac{R}{R_c})\alpha]^{-1}$ .<sup>4</sup> For the unpinned data in Fig. 5, we find  $\alpha = 0.007$ , which is typical for  $\text{Ni}_{80}\text{Fe}_{20}$ . For the core that becomes pinned (Fig. 5),  $\alpha$  is essentially the same for  $t < 30$  nsec, but the apparent damping increases as the core becomes pinned. This is unlikely, however, to reflect a true increase in the damping rate. The simulations of Min *et al.*<sup>27</sup> suggest that the effect of pinning on the damping rate should be small. It is more likely that fluctuations in the phase of the core motion relative to the optical probe pulse become larger as the core orbit encloses fewer pinning sites, leading to the apparent increase in the damping rate. In the absence of a single-shot measurement, it is impossible to rule out such a mechanism.

In summary, linear and non-linear regimes of vortex dynamics are identified in a single magnetic disk over a large dynamic range in drive amplitude. The spectra reveal transitions between different dynamical regimes. Data in both the frequency and time domains are used to develop a quantitative model of the pinning potential, an approach that can be generalized to other simple domain structures. The observation of hysteresis while sweeping the rf field provides a demonstration of metastable gyrotropic orbits in a phase space of drive amplitude and frequency. This complete picture of vortex dynamics in the presence of pinning will facilitate further development of spintronic devices that contain vortices or vortex domain walls.

This work was supported primarily by the MRSEC Program of the National Science Foundation under Award Number DMR-0819885. Additional support was provided by a University of Minnesota Doctoral Dissertation Fellowship, and use of the U of M Nanofabrication Center was supported by the NSF NNIN network. The authors thank Chris Leighton and Rob Compton for assistance in sample fabrication.

- 
- \* [crowell@physics.umn.edu](mailto:crowell@physics.umn.edu)
- <sup>1</sup> B. E. Argyle, E. Terrenzio, and J. C. Slonczewski, *Phys. Rev. Lett.* **53**, 190 (1984).
  - <sup>2</sup> J. P. Park, P. Eames, D. M. Engebretson, J. Berezovsky, and P. A. Crowell, *Phys. Rev. B* **67**, 020403 (2003)(R).
  - <sup>3</sup> S.-B. Choe, Y. Acremann, A. Scholl, A. Bauer, A. Doran, J. Stöhr, and H. A. Padmore, *Science* **304**, 420 (2004).
  - <sup>4</sup> K. Y. Guslienko, B. A. Ivanov, V. Novosad, Y. Otani, H. Shima, and K. Fukamichi, *J. Appl. Phys.* **91**, 8037 (2002).
  - <sup>5</sup> J. P. Park and P. A. Crowell, *Phys. Rev. Lett.* **95**, 167201 (2005).
  - <sup>6</sup> V. Novosad, F. Y. Fradin, P. E. Roy, K. S. Buchanan, K. Y. Guslienko, and S. D. Bader, *Phys. Rev. B* **72**, 024455 (2005).
  - <sup>7</sup> K. S. Buchanan, M. Grimsditch, F. Y. Fradin, S. D. Bader, and V. Novosad, *Phys. Rev. Lett.* **99**, 267201 (2007).
  - <sup>8</sup> K. Y. Guslienko, R. H. Heredero, and O. Chubykalo-Fesenko, *Phys. Rev. B* **82**, 014402 (2010).
  - <sup>9</sup> K. Y. Guslienko, K.-S. Lee, and S.-K. Kim, *Phys. Rev. Lett.* **100**, 027203 (2008).
  - <sup>10</sup> A. Vansteenkiste *et al.*, *Nat. Phys.* **5**, 332 (2009).
  - <sup>11</sup> B. Van Waeyenberge *et al.* *Nature* **444**, 461 (2006).
  - <sup>12</sup> K. Yamada, S. Kasai, Y. Nakatani, K. Kobayashi, H. Kohono, A. Thiaville, and T. Ono, *Nat. Mater.* **6**, 270 (2007).
  - <sup>13</sup> M. Weigand *et al.* *Phys. Rev. Lett.* **102**, 077201 (2009).
  - <sup>14</sup> B. Pigeau, G. de Loubens, O. Klein, A. Riegler, F. Lochner, G. Schmidt, and L. W. Molenkamp, *Nat. Phys.* **7**, 26 (2011).
  - <sup>15</sup> R. L. Compton and P. A. Crowell, *Phys. Rev. Lett.* **97**, 137202 (2006).
  - <sup>16</sup> V. S. Pribyl, I. N. Krivorotov, G. D. Fuchs, P. M. Braganca, O. Ozatay, J. C. Sankery, D. C. Ralph, and R. A. Buhrman, *Nat. Phys.* **3**, 498 (2007).
  - <sup>17</sup> R. L. Compton, T. Y. Chen, and P. A. Crowell, *Phys. Rev. B* **81**, 144412 (2010).
  - <sup>18</sup> T. Y. Chen and P. A. Crowell, *IEEE Trans. Magn.* **46**, 1457 (2010).
  - <sup>19</sup> J.-S. Kim *et al.* *Phys. Rev. B* **82**, 104427 (2010).
  - <sup>20</sup> A. Dussaux *et al.* *Nat. Commun.* **1**, 1 (2010).
  - <sup>21</sup> G. S. D. Beach, C. Nistor, C. Knutson, M. Tsoi, and J. L. Erskine, *Nat. Mater.* **4**, 741 (2005).
  - <sup>22</sup> D. Bedau, M. Kläui, M. T. Hua, S. Krzyk, U. Rüdiger, G. Faini, and L. Vila, *Phys. Rev. Lett.* **101**, 256602 (2008).
  - <sup>23</sup> R. Moriya, L. Thomas, M. Hayashi, Y. B. Bazaliy, C. Rettner, and S. S. P. Parkin, *Nat. Phys.* **4**, 368 (2008).
  - <sup>24</sup> W. K. Hiebert, A. Stankiewicz, and M. R. Freeman, *Phys. Rev. Lett.* **79**, 1134 (1997).
  - <sup>25</sup> A. A. Thiele, *Phys. Rev. Lett.* **30**, 230 (1973).
  - <sup>26</sup> See Supplemental Material at [URL will be inserted by publisher] for the description of the double modulation technique.
  - <sup>27</sup> H. Min, R. D. McMichael, J. Miltat, and M. D. Stiles, *Phys. Rev. B* **83**, 064411 (2011).